HHS Public Access

Author manuscript

Cancer Immunol Res. Author manuscript; available in PMC 2021 December 09.

Published in final edited form as:

Cancer Immunol Res. 2021 August ; 9(8): 877–890. doi:10.1158/2326-6066.CIR-20-0785.

Site-dependent immune escape due to impaired dendritic cell cross-priming

Mark S. Diamond[1,2], **Jeffrey H. Lin**[2,3], **Robert H. Vonderheide**[1,2]

[1]Division of Hematology Oncology, Department of Medicine, Perelman School of Medicine, University of Pennsylvania, Philadelphia, Pennsylvania, USA.

[2]Abramson Cancer Center, University of Pennsylvania, Philadelphia, Pennsylvania, USA.

[3]Immunology Graduate Group, Perelman School of Medicine, University of Pennsylvania, Philadelphia, Pennsylvania, USA.

Abstract

T-cell recognition of tumor neoantigens is critical for cancer immune surveillance and the efficacy of immunotherapy. Tumors can evade host immunity by altering their antigenicity or orchestrating an immunosuppressive microenvironment, leading to outgrowth of poorly immunogenic tumors through the well-established process of cancer immunoediting. Whether cancer immune surveillance and immunoediting depends on the tissue site of origin, however, is poorly understood. Herein, we studied T cell-mediated surveillance of antigenic, clonal murine pancreatic adenocarcinoma cells expressing neoantigen. Whereas such tumors are robustly eliminated after subcutaneous or intravenous challenge, we observed selective immune escape within the pancreas and peritoneum. Tumor outgrowth occurred in the absence of immunoediting, and antitumor immunity could not be rescued by PD-1 or CTLA-4 checkpoint blockade. Instead, tumor escape was associated with diminished $CD8^+$ T-cell priming by type I conventional dendritic cells (cDC1s). Enhancing cDC1 cross-presentation by CD40 agonist treatment restored immunologic control by promoting T-cell priming and broadening T-cell responses through epitope spread. These findings demonstrate that immune escape of highly antigenic tumors can occur without immunoediting in a tissue-restricted manner and highlight barriers to cDC1-mediated T-cell priming imposed by certain microenvironments that must be addressed for successful combination immunotherapies.

Keywords

Immune surveillance; immunoediting; antigenicity; immune escape; neoantigen

Introduction

Cancer immunotherapies augmenting endogenous antitumor T cells have demonstrated remarkable clinical benefit in certain cancers, yet the majority of patients remain refractory

Corresponding author: Robert H. Vonderheide, 12 South Pavilion, 3400 Civic Center Blvd, Philadelphia, Pennsylvania, 19104. Phone: (215) 662-3929. rhv@upenn.edu.

to current approaches (1,2). Understanding the determinants of tumor immunogenicity is therefore essential, particularly for solid tumors that often exhibit sparse T-cell infiltration and primary resistance to immune checkpoint inhibitors (ICIs) targeting the PD-1/PD-L1 and/or CTLA-4 pathways. Whereas tumor antigens are clear requisites for immune recognition, the contribution of the microenvironment on cancer immune surveillance is less well understood.

Formative studies using murine sarcoma models have established the capacity of innate and adaptive immunity to modulate primary tumor development and sculpt the immunogenicity of developing tumors (3,4). Neoantigens generated by cancer-specific mutations and recognizable as foreign by T cells are central targets of immune surveillance and immunoediting in such models (5,6). Neoantigen-specific T cells are also critical for ICI-mediated responses against less immunogenic tumors (7,8). In cancer patients, tumor mutational burden similarly correlates with ICI response in several malignancies (9,10), and loss of neoantigen expression or deficits in antigen presentation, including the loss of interferon sensitivity, have been detected in tumors with primary or acquired immunotherapy resistance (11–13).

Tumor antigenicity alone, however, is insufficient to predict ICI response, and important biomarkers related to the tumor microenvironment (TME) have also been identified, including $CD8^+$ T-cell infiltration, expression of T cell-inflamed genes, PD-L1 staining, and other markers of ongoing immune reactivity (14,15). However, the correlation is poor across cancer types between an inflamed TME and tumor mutational burden or the density of immunogenic antigens (10,16,17). This dissociation between tumor antigenicity and immunogenicity is likely multifactorial and consistent with the influence of both tumor cell-intrinsic and extrinsic factors actively modulating the immune landscape. Various relevant pathways have indeed emerged, including checkpoint molecules or immunosuppressive cytokines downstream of oncogenic signaling, and host-related factors such as immune status or the microbiome (18–21). Interestingly, mixed clinical responses to ICI are sometimes observed within the same patient, and reduced ICI efficacy for tumors at certain anatomic sites has been reported (22,23). These observations have largely been understood in the context of tumor heterogeneity or differences in tumor-intrinsic immunosuppression (24–26), though preclinical studies also raise the possibility of differential cancer surveillance based on tissue site of origin (27–29).

Pancreatic ductal adenocarcinoma (PDAC) is an extremely lethal cancer with a particularly immunosuppressive TME, characterized by poor $CD8^+$ T-cell infiltration (immunologically ‘cold’) and ICI unresponsiveness (30–32). Yet, human PDAC contains mutational and genomic complexity (33), increased T-cell infiltration is associated with better prognosis (34), and T-cell reactivity to high quality neoantigens was discovered in rare long-term PDAC survivors (35), suggesting promise for immunotherapy if barriers can be surmounted. Genomic and transcriptional analyses of human PDAC, however, have suggested that cytolytic activity does not correlate with increased mutational or neoepitope load (36) as noted in some cancers (37), and various tumor-intrinsic immunosuppressive mechanisms have been characterized in preclinical models of this disease (38–40).

Using the 'KPC' genetically-engineered murine model (GEMM) of PDAC, driven by pancreatic expression of mutant Kras and p53, we previously demonstrated that T-cell depletion does not affect the natural history of tumor development (41) – a finding in contrast to carcinogen-induced tumor models or more immunogenic GEMMs (4,6). KPC-derived tumors had a low mutational burden and few predicted neoepitopes, and introduction of a single neoantigen could reestablish protective immunity and elicit immunoediting (41), leading to the hypothesis that immune quiescence in PDAC arises from low tumor antigenicity. In the current study, we explored T cell-mediated surveillance of neoantigen-expressing PDAC, finding that high tumor antigenicity is not sufficient within certain host tissue microenvironments, including the pancreas. Instead, we observed differential immune surveillance and escape of antigenic tumors without immunoediting, a consequence of poor immune priming, which could be restored by enhancing dendritic cell (DC) function.

Materials and Methods

Mice.

Wild-type (WT) C57BL/6J mice were purchased from The Jackson Laboratory. *Rag2*$^{-/-}$, μMT, Act-mOVA, *Batf3*$^{-/-}$, *CD40*$^{-/-}$, *Lta*$^{-/-}$, and *Cxcr3*$^{-/-}$ mice on a C57BL/6 background were obtained from The Jackson Laboratory and/or bred at the University of Pennsylvania. For tumor transplantation experiments, generally female mice at approximately 8–12 weeks of age were used. Mice were maintained in a specific pathogen-free barrier facility in accordance with American Association for Laboratory Animal Science guidelines. All study protocols involving mice were approved by the University of Pennsylvania Institutional Animal Care and Use Committee.

Tumor cells.

The 4662 PDAC cell line was derived from a spontaneous pancreatic adenocarcinoma in a female KPC (Kras$^{LSL\text{-}G12D/+}$Trp53$^{LSL\text{-}R172H/+}$Pdx-Cre$^{+/-}$) mouse on the C57BL/6J background (42), and the presence of rearranged *Kras* and *Trp53* alleles were verified by RT-PCR (41). Cells were tested by the Research Animal Diagnostic Laboratory (RADIL) at the University of Missouri using the Infectious Microbe PCR Amplification Test (IMPACT) and regularly screened for mycoplasma. Cells from a low-passage stock were used, and no re-authentication was performed. The 4662 tumor line (referred to herein as simply parental PDAC) was cloned by limiting dilution to generate the parental clones C9 and C10, or transduced with a retroviral construct containing full-length ovalbumin fused to Td-tomato and cloned to generate V6.Ova and G10.Ova as described (41). The V6.Ova clone was used for subsequent studies unless otherwise indicated, and is referred to as PDAC.Ova. Tumor cell lines were generated from primary tumors by digesting with collagenase type IV (1 mg/mL; Sigma-Aldrich) in DMEM for 45 minutes at 37ºC and frozen down as low-passage cell lines after several *in vitro* passages to eliminate contaminating immune cells and fibroblasts. Cells were grown in D10 media containing DMEM (Gibco) plus 10% FBS (Gemini), 2mM L-glutamine (BioWhittaker), and gentamicin (80 μg/mL; Gibco). For *in vitro* growth assays, cells were plated at 1.25×10^5 cells per T25 flask, and triplicate samples were harvested by trypsinization at the indicated time points and counted using a coulter counter.

Tumor implantation.

Tumor cells were harvested by trypsinization at approximately 60–90% confluence, washed with DMEM, and counted using a hemacytometer. The viability of injected cells was >90% as assessed by trypan blue exclusion. For subcutaneous (s.c.) implant studies, tumor cells were injected in 100 μL DMEM using a 27-gauge 1.0cc TB syringe into the shaved flanks of mice. Tumor size was measured in two orthogonal diameters using a ruler every 4 days and plotted as mean tumor diameter. Mice were euthanized for tumor diameters approaching 20 mm or significant tumor ulceration. For orthotopic implant studies, tumor cells were injected into the tail of the pancreas in 25 μL DMEM using a 29-gauge 0.3cc insulin syringe, with visualization of a small fluid bubble to indicate successful injection without leakage. Mice were anesthetized with 1–3% isoflurane, laparotomy performed using sterile surgical technique, and the spleen and pancreatic tissue externalized prior to injection. The peritoneum was closed using absorbable Polymend MT 5/0 suture (Penn Veterinary Supply) and the overlying skin with wound clips. Tumor size was quantitated weekly, or as indicated, by 3-dimensional ultrasonography using the Vevo 2100 imaging system with a 55-MHz MicroScan transducer (Visual Sonics). Mice were euthanized for tumor volumes approaching 1200 mm^3 or moribund condition. For intraperitoneal (i.p.) implants, tumor cells were injected in 250 μL total volume using a 27-gauge 1.0cc TB syringe. For intravenous (i.v.) implants, tumor cells were injected via retroorbital injection in 100 μL PBS containing 2mM EDTA (to minimize cell clumping) using a 29-gauge 0.5cc insulin syringe. Oral tolerance to ovalbumin was induced in WT mice by oral gavage with 50 mg ovalbumin protein (Sigma-Aldrich) in 250 μL PBS weekly for three doses as described (41), followed one week later by implantation of tumor cells. For retransplant experiments, ‘escape’ or control ‘passage’ tumor lines were injected s.c. into WT mice as above, and mice with progressively growing tumors >5 mm diameter by day 40 were considered tumor positive. For tumor rechallenge experiments, mice that had completely rejected s.c. PDAC.Ova tumors (>50 days from injection) were challenged with orthotopic or i.p. tumor cells. For Ova^+ and Ova^- tumor cell mixing experiments, a total of 1×10^6 cells at the indicated ratio were injected. Mice challenged with parental PDAC after PDAC.Ova priming had been injected s.c. with PDAC.Ova on the opposite flank 40 days prior and treated at day 7 with control Ig or CD40 agonist.

Antibody treatment.

For T-cell depletion, monoclonal anti-CD8 (2.43) and/or monoclonal anti-CD4 (GK1.5) were injected i.p. at a dose of 0.2 mg every 4 days, starting 1–3 days prior to tumor challenge or CD40 agonist treatment as indicated. NK-cell depletion was achieved by injection of 0.2 mg monoclonal anti-NK1.1 (PK136) on days −2, 0, 2, then every 5 days relative to tumor injection. CD40 agonist (FGK45) was administered as a single dose of 0.1 mg i.p. on day 7 or day 12 relative to tumor challenge. Control Igs (LTF-2 or 2A3) were used at comparable dosing schedules. Anti-PD-1 (RMP1–14) and anti-CLTA-4 (9H10) blocking antibodies were administered i.p. at 0.2 mg every 3 days for 3 doses as indicated. All antibodies were obtained from BioXCell as low endotoxin preparations. Cell depletions using the indicated treatment regimens were confirmed by flow cytometry.

Flow cytometry.

Single-cell suspensions were prepared from tumors, lymph nodes, or spleens by finely mincing tissue and digesting with 1 mg/mL collagenase type IV (Sigma-Aldrich) for 45–60 minutes at 37ºC. Tumor-draining lymph nodes were isolated using a dissecting microscope. Cells grown *in vitro* were harvested by trypsinization, and in some cases treated with recombinant murine IFNγ (R&D systems) at 100 U/mL for 48 hours prior to analysis. Live/dead cell discrimination was achieved using Live/Dead Fixable Aqua stain (Invitrogen). For H-2K^b-SIINFEKL tetramer staining, cells were incubated with PE-conjugated H-2K^b Ova (SIINFEKL) tetramer or negative control tetramer (MBL International) for 10–15 minutes at 37ºC prior to surface marker staining, which was performed for 30 minutes at 4ºC. For intracellular staining, fixation and permeabilization were performed using the eBioscience Foxp3/transcription factor staining buffer kit. The following reagents were obtained from BioLegend: H-2K^b-FITC or -PerCP/Cy5.5 (AF6–88.5), H-2D^b-biotin (KH95), H-2K^b-SIINFEKL-APC (25-D1.16), CD31-APC (MEC13.3), CD3-FITC (145–2C11), CD4-APC (RM4–5), CD8α-PE/Cy7 (53–6.7), TCRγ/δ-FITC or -PE/Cy7 (GL3), NK1.1-PE/Cy7 or -BV711 (PK136), CD49b-FITC (DX5), NKp46-PE (29A1.4), CD62L-PE/Cy7 or -APC/Cy7 (MEL-14), F4/80-FITC or -APC/Cy7 (BM8), Gr-1-APC/Cy7 or -BV711 (RB6–8C5), CD103-APC or -BV421 (2E7), PD-1-PE/Cy7 or -APC/Cy7 (29F.1A12), granzyme B-AF647 or -APC (GB11), and T-bet-BV421 (4B10), LAG-3-PerCP/Cy5.5 (C9B7W), CTLA-4-PE-CF594 (UC10–4B9), CD45-AF700 (30-F11), Ki-67-BV605 (16A8), CD3-BV711 (17A2), CD44-BV785 (IM7), XRC1-FITC (ZET), I-A/I-E-APC (M5/114.15.2), CD11c-BV605 (N418), CD80-BV650 (16–10A1), CD19-BV711 (6D5), B220-BV711 (RA3–6B2), CD86-BV785 (GL-1), CD40-PE (3/23), CD64-PE-CF594 (X54–5/7.1), CD11b-PE/Cy5 (M1/70), and SIRPα-PE/Cy7 (P84). The following were from BD Biosciences: streptavidin-V450, CD45-PerCP (30-F11), CD4-V450 (RM4–5), CD4-BUV395 (GK1.5), CD8α-APC/Cy7 or -BUV805 (53–6.7), CD3ε-V450 (500A2), CD44-FITC (IM7), CD11b-V450 (M1/70), CD11c-PE (HL3), and CD90.2-BV650 (30-H12), and CD274-BUV395 (MIH5). The following were from eBioscience: Foxp3-PE or -APC (FJK-16s), TIM-3-FITC (RMT3–23), and Eomes-PE/Cy5 (Dan11mag). Data was acquired on a FACSCanto or LSR Fortessa flow cytometer (BD Biosciences) and analyzed using FlowJo software (FlowJo, LLC). Analysis of cDC subsets was performed using a gating strategy as previously described (43), with markers including CD45, CD64, F4/80, MHC-II, lineage markers (CD3, CD19, B220, NK1.1, and Gr-1), CD11c, XCR1, and SIRPα, as well as CD103, CD11b, and CD8α where applicable.

Histopathology.

Tumor and lung tissues were harvested and immediately fixed in zinc formalin (Sigma-Aldrich) by intratracheal instillation of fixative. Sectioning and standard hematoxylin and eosin (H&E) staining was performed by the Pathology Core Lab at the Children's Hospital of Philadelphia Research Institute. Images were acquired using a Nikon DS-Fi2 digital microscope camera.

Statistical analysis.

Significance of Kaplan-Meier survival curves was determined by log-rank (Mantel-Cox) test. Flow data was compared by one-way ANOVA with Tukey's post-hoc test, unpaired t test, or Mann-Whitney test. Statistical analyses were performed using GraphPad Prism.

Results

Immune escape of antigenic PDAC

To evaluate T-cell immune surveillance within different microenvironments, we employed clonal KPC-derived murine PDAC cells engineered to have high antigenicity by enforced expression of the model antigen ovalbumin (Ova) fused to td-Tomato (PDAC.Ova) (Supplementary Fig. S1A). Parental PDAC and PDAC.Ova lines displayed similar growth kinetics *in vitro* and *in vivo* in immunodeficient *Rag2*$^{-/-}$ mice, neoantigen expression was stable over time, and tumors exhibited similar morphologies *in vivo* (Supplementary Fig. S1B-E). Although parental PDAC grew progressively in syngeneic WT hosts, PDAC.Ova was readily eliminated after s.c. transplant into immunocompetent mice (Fig. 1A-C, Supplementary Fig. S1F), consistent with our prior results (41). Rejection of PDAC.Ova required CD8^{+} T lymphocytes, but not B cells or NK cells, and tumor rejection was abrogated in mice with specific immunologic tolerance to Ova (Act-mOVA transgenic mice) (Fig. 1C) (41). In contrast to the uniform rejection of s.c. PDAC.Ova cells, orthotopic intrapancreatic challenge revealed reproducible outgrowth in a subset of WT hosts (Fig. 1D), with approximately 30% (7/24 mice) tumor growth over multiple experiments compared to no tumor outgrowth (0/25 mice) with s.c. transplantation. Rejection of orthotopic PDAC.Ova similarly required CD8^{+} T cells and was not observed in Act-mOVA mice (Fig. 1D) or upon induction of Ova tolerance in WT mice by serial oral gavage (Supplementary Fig. S2A-C). Control of orthotopic PDAC.Ova tumors was potentially enhanced in μMT mice (Fig. 1D), consistent with a pro-tumorigenic role of B cells in PDAC (44,45), although larger group sizes are needed for more conclusive assessment. At higher cell inoculums, PDAC.Ova grew progressively in the majority of WT mice following orthotopic implantation (75%, 9/12 mice), but only rarely following s.c. injection (12%, 3/25 mice) (Fig. 1E-F).

When we tested tumor growth following i.p. injection, we found that PDAC.Ova was lethal in WT mice, even at low cell inoculums, with kinetics similar to the parental line (Fig. 1G-H). Alternatively, i.v. injection of parental PDAC cells induced multiple lung metastases in WT mice, whereas PDAC.Ova cells did not (Fig. 1G-H, Supplementary Fig. S2D), unless injected into tolerant Act-mOVA hosts (Supplementary Fig. S2D-E). Thus, the outgrowth of PDAC.Ova cells in immunocompetent WT mice depended on the site of tumor implantation (Fig. 1H), but parental PDAC cells were generally lethal regardless of route (Fig. 1G). Similar results were also obtained with two clonal cell lines derived from the parental tumor and an additional PDAC.Ova tumor clone (Supplementary Fig. S1A and S1F). These data reveal that the immunogenicity of clonal PDAC.Ova cells is shaped by the host tissue microenvironment, with selective immune escape of an antigenic tumor in the pancreas and peritoneum.

Tumor outgrowth is not due to neoantigen loss

To determine whether outgrowth of PDAC.Ova tumors reflected loss of neoantigen, we harvested orthotopic or i.p. tumors from WT mice and generated low-passage cell lines (termed orthotopic or i.p. 'escapes'). As a control, PDAC.Ova lines were established from orthotopic tumors in WT mice treated with depleting anti-CD8 ('αCD8-passage'). By flow cytometry, orthotopic and i.p. 'escape' tumors retained expression of td-Tomato, presented the Ova-derived SIINFEKL peptide in the context of H-2K^b, and upregulated MHC class I molecules (H-2K^b and H-2D^b) upon treatment with IFNγ (Fig. 2A-C). When retransplanted s.c. into naïve WT mice, orthotopic 'escape' and 'αCD8-passage' tumors were still rejected in the majority of WT mice, but grew in T cell-depleted hosts, and growth kinetics were comparable in 'escape' and 'αCD8-passage' tumors (Fig. 2D-E), although both groups were slightly more tumorigenic than the original PDAC.Ova at an equivalent cell dose (likely attributable to *in vivo* passage). These data are therefore consistent with a failure in antitumor immunity leading to escape, rather than tumor-intrinsic immunoediting.

T-cell priming defect underlies immune escape

To examine the immune response against PDAC.Ova, we analyzed the priming of tumor-specific SIINFEKL-H-2K^b tetramer$^+$ (Ova tet$^+$) T cells and tumor-infiltrating leukocyte (TIL) populations by flow cytometry. Compared to early s.c. PDAC tumors at day 9, PDAC.Ova tumors in WT mice had increased total T-cell infiltration, particularly CD8$^+$ T cells, which was not observed in Act-mOVA mice or WT mice with induced oral tolerance to Ova (Fig. 3A, Supplementary Fig. S3A-C). There was an associated decrease in CD11b$^+$ myeloid cells, including both CD11b$^+$Gr-1^{hi} and F4/80$^+$ subsets (Supplementary Fig. S3D). As expected, we found a significant expansion of Ova tet$^+$ T cells in the spleens of WT mice following s.c. challenge with PDAC.Ova, but this was largely absent in Act-mOVA mice or WT mice treated with Ova gavage (Fig. 3B). When we assessed T-cell priming following i.p. or orthotopic implantation of PDAC.Ova, we found diminished expansion of Ova tet+ T cells in the spleen compared to s.c. challenge (Fig. 3B). More robust CD8$^+$ T-cell priming was observed in a subset of mice following orthotopic injection, which correlated with the absence of detectable tumor upon harvest at day 12–14 (Fig. 3C). In i.p. challenged mice, initial expansion of Ova tet$^+$ CD8$^+$ T cells in the spleen was attenuated at multiple early time points (Fig. 3D).

Analysis of progressively growing i.p. PDAC.Ova tumors harvested from WT mice showed that CD8$^+$ and CD4$^+$ T-cell infiltration was comparable to i.p. parental PDAC tumors (Fig. 3E, Supplementary Fig. S3E-F), and relatively few infiltrating Ova tet$^+$ CD8$^+$ T cells were detected in PDAC.Ova tumors (Fig. 3B). NK cell and myeloid cell infiltration within PDAC and PDAC.Ova tumors was also similar (Supplementary Fig. S3G). Harvest of orthotopic PDAC.Ova tumors from WT mice also revealed T-cell infiltration comparable to orthotopic parental PDAC tumors and low relative abundance of Ova tet$^+$ T cells in the spleen (Supplementary Fig. S4A-C). In contrast to i.p. PDAC.Ova tumors, higher levels of Ova-specific CD8$^+$ T cells accumulated within established orthotopic PDAC.Ova tumors, at least in a subset of mice (Fig. 3B). Collectively, these findings demonstrate diminished CD8$^+$ T-cell priming and reduced immunogenicity of PDAC.Ova in the peritoneal and pancreatic microenvironments.

We next performed phenotypic studies to examine the $CD8^+$ T cells infiltrating s.c. PDAC.Ova compared to progressively growing i.p. and orthotopic PDAC.Ova. $CD8^+$ T cells in s.c. PDAC.Ova tumors largely displayed an effector phenotype, with increased expression of activation markers and effector molecules such as CD44, PD-1, T-bet, and granzyme B, in comparison to $CD8^+$ T cells from s.c. parental PDAC (Fig. 3F, Supplementary Fig. S4D). In contrast, $CD8^+$ TILs from i.p. and orthotopic PDAC.Ova tumors lacked expression of effector molecules and exhibited elevated PD-1 and TIM-3 (Fig. 3F, Supplementary Fig. S4E-F), raising the possibility of T-cell exhaustion, although *ex vivo* functional assessment would be required to evaluate this possibility.

Finally, we hypothesized that low abundance or impaired maturation of cDCs within i.p. or orthotopic PDAC.Ova compared to s.c. tumors might result in poor T-cell priming. We thus examined cDC subsets in the tumor and tumor-draining lymph node (dLN) by flow cytometry, enumerating $XCR1^+$ cDC1s and $SIRP\alpha^+$ cDC2s, among cDCs defined as $CD45^+CD64^-MHCII^+CD11c^+$ cells lacking expression of lineage markers CD3, CD19, B220, NK1.1, and Gr-1, as described (43). Such analyses, however, did not reveal a reduction in total cDCs or cDC1s in the tumor or dLN correlating with impaired antitumor immunity (Fig. 3G-H). Maturation markers, including CD40, CD80, CD86, PD-L1, and MHC-II, on cDC1s were also not substantially altered based on site of PDAC.Ova implantation or between parental PDAC and PDAC.Ova tumors growing at the same anatomic site (Supplementary Fig. S5).

cDC1s and host CD40 are required for T-cell priming

Given the central function for *Batf3*-dependent cDC1s in antigen cross-presentation (46) and the CD40 pathway for $CD4^+$ T cell-mediated DC licensing (28,47), we evaluated T-cell priming in $Batf3^{-/-}$ and $CD40^{-/-}$ mice. Compared to robust expansion of Ova tet^+ T cells in WT mice bearing s.c. PDAC.Ova, the absence of cDC1s nearly completely blocked early $CD8^+$ T-cell priming (Fig. 4A). In $CD40^{-/-}$ hosts, tumor infiltration by Ova-specific $CD8^+$ T cells was significantly reduced but not eliminated (Fig. 4A). Similar experiments also confirmed the importance of cDC1s and CD40 in T-cell priming against tumors following i.p. challenge (Fig. 4B). These data correlated with tumor outgrowth following s.c. or orthotopic challenge, as PDAC.Ova tumors grew in $Batf3^{-/-}$ mice with kinetics similar to $CD8^+$ T cell-depleted mice (Fig. 4C-E). PDAC.Ova tumors also grew progressively in subsets of $CD40^{-/-}$ mice, although the phenotype appeared more substantial following orthotopic compared to s.c. implantation (Fig. 4C-E). Following orthotopic PDAC.Ova injection, there was minimal Ova tet^+ T-cell expansion or tumor infiltration at later time points in $CD40^{-/-}$ mice with progressively growing tumors, comparable to Ova-tolerant hosts (Supplementary Fig. S4B). Accumulation of Ova tet^+ T cells did occur, however, in the spleen and late orthotopic PDAC.Ova tumors in a subset of $Batf3^{-/-}$ mice (Supplementary Fig. S4B-C), indicating that other APCs could prime $CD8^+$ T cells in the absence of cDC1s; however, T cells lacked an effector phenotype (Supplementary Fig. S4E-F).

Prior work has suggested that cDC production of CXCR3 chemokines is required for optimal T-cell infiltration (48,49) and that NK cells promote cDC recruitment to the TME (50). We therefore investigated the growth of s.c. and orthotopic PDAC.Ova in NK cell-

depleted WT mice or in *CXCR3*$^{-/-}$ hosts. In both cases, we found that tumor rejection and survival was similar to WT mice (Fig. 4F-H) and that Ova tet^{+} CD8^{+} T-cell expansion or tumor infiltration was unchanged in the absence of NK cells or host CXCR3 (Fig. 4A). We confirmed effective depletion of NK cells in the TME and observed TIL profiles similar to WT mice, with increased CD8^{+} T-cell infiltration and reduced myeloid populations (Supplementary Fig. S3A-D). Growth of PDAC.Ova in lymphotoxin alpha-deficient (*Lta*$^{-/-}$) mice, which lack secondary lymphoid tissues (51), confirmed the importance of lymph nodes for immune priming and PDAC.Ova rejection (Fig. 4C-E). These data therefore indicate that the essential function of cDC1s relates largely to T-cell priming rather than lymphocyte recruitment and that antitumor immunity in this model occurs independently of NK cells.

We also asked whether CD4^{+} T-cell help was required for immune responses to s.c. and orthotopic PDAC.Ova tumors. Cohorts of WT mice were challenged with low-dose PDAC.Ova via s.c. or orthotopic injection and treated with control Ig or depleting anti-CD4 or anti-CD8. Rejection of s.c. PDAC.Ova tumors was dependent on CD8^{+} T cells but independent of CD4^{+} cells (Supplementary Fig. S6A-B), consistent with our prior results that also included high-dose s.c. challenge (41). In contrast, rejection of orthotopic PDAC.Ova tumors after low-dose challenge was completely dependent on CD4^{+} cells (Supplementary Fig. S6C-D), and in a subset of animals, delayed tumor escape was observed in the absence of CD4^{+} T-cell help. These findings reveal distinct immunologic requirements for tumor control at different anatomic sites and suggest that a more coordinated immune response is required within the pancreatic TME, although the precise contribution of CD4^{+} T cells in the setting of orthotopic PDAC.Ova tumors remains unclear.

Protection by antecedent but not concurrent PDAC.Ova

We next investigated whether prior T-cell priming could protect mice against subsequent orthotopic or i.p. PDAC.Ova implantation. Mice that had previously rejected PDAC.Ova cells via s.c. injection displayed complete protection against high-dose orthotopic or i.p. tumor rechallenge (Fig. 5A-C), whereas PDAC.Ova grew in the majority of naïve WT mice. The timing of s.c. priming relative to i.p. injection was important, as neither concurrent s.c. and i.p. injection nor delayed s.c. injection (one week after i.p. injection) were protective (Fig. 5D); yet, s.c. injection a week prior to i.p. challenge prevented lethality (Fig. 5D). In concurrently challenged mice, s.c. tumors were eliminated in most mice, despite progressive growth of PDAC.Ova within the peritoneum (Fig. 5E). When we assessed Ova-specific CD8^{+} T-cell expansion in the spleen at the height of the response on day 9, we found that priming in the s.c. and i.p. concurrently injected mice was slightly increased over i.p. alone but not significantly (Fig. 5F). Similarly, there was a trend toward reduced tumor infiltration by Ova tet^{+} T cells into the s.c. tumors of concurrently injected mice (Fig. 5G). These data indicate that the presence of i.p. PDAC.Ova tumors inhibited protective antitumor priming with s.c. injection, whereas in concurrently injected animals, perhaps a lower threshold for immune reactivity still permitted tumor control at the s.c. site.

CD40 agonist, but not checkpoint blockade, prevents PDAC.Ova escape

We hypothesized that augmenting APC function through CD40 agonist administration might enhance T-cell priming and restore antitumor immunity against intrapancreatic and i.p. PDAC.Ova. We therefore challenged mice with orthotopic PDAC.Ova, followed by treatment on day 7 with a single dose of either control Ig or anti-CD40 agonist. Although tumors grew progressively in most control-treated mice, CD40 agonist-treated mice uniformly rejected this tumor challenge (Fig. 6A-B). We confirmed that the CD40 agonist was acting on host cells because its effect was lost in *CD40*$^{-/-}$ mice (Fig. 6A-B). We established that T cells were required for the efficacy of anti-CD40, as T-cell depletion abrogated its protective effect (Fig. 6A-B). Similar results were also obtained when mice were challenged with PDAC.Ova tumor cells via i.p. implantation (Fig. 6C). The efficacy of CD40 agonist monotherapy required the presence of neoantigen, as anti-CD40 treatment of WT mice injected with PDAC cells either had no effect (i.p. challenge) or led to a modest but significant delay in tumor growth but no regressions (orthotopic challenge) (Supplementary Fig. S7).

We subsequently explored whether enhancing T-cell function through blockade of PD-1 or CTLA-4 inhibitory receptors could prevent PDAC.Ova escape. Mice challenged with orthotopic PDAC.Ova were treated at day 12 with control Ig, single-dose CD40 agonist, or serial anti-PD-1 (3 doses, q3 days). Whereas the CD40 agonist was protective and induced rejection of intrapancreatic tumors, we observed poor efficacy of PD-1 blockade (Fig. 6D-E). We obtained similar results upon treatment of i.p. PDAC.Ova tumors with control Ig, anti-CD40, or anti-PD-1 (Fig. 6F). Orthotopic PDAC.Ova tumors harvested from anti-PD-1-treated mice showed no evidence of neoantigen or MHC class I loss as a mechanism of escape, and PD-L1 expression was similar (Supplementary Fig. S8). If mice challenged with i.p. PDAC.Ova were instead treated with serial anti-CTLA-4 starting at day 6–7 (3 doses, q3 days), we observed partial protection (Fig. 6G), consistent with the capacity of CTLA-4 blockade to also promote T-cell expansion (7). However, anti-CTLA-4 treatment displayed significantly less efficacy than the single-dose of CD40 agonist, underscoring the importance of APC activation through the CD40 pathway. These findings demonstrate that the immunosuppressive TME within the pancreas and peritoneum can be overcome by enhancing CD40 signaling, yet blockade of T-cell inhibitory receptors alone was not sufficient to prevent PDAC.Ova escape.

CD40 activation enhances T-cell cross-priming by cDC1s

To understand the mechanism of action of CD40 agonism, we measured tumor-specific CD8^{+} T cells in the spleens of mice challenged with i.p. PDAC.Ova tumor cells. Compared to control Ig-treated mice in which T-cell priming remained poor, we observed a significant expansion of Ova tet^{+} T cells following CD40 agonist-treatment (Fig. 6H), consistent with enhanced CD8^{+} T-cell priming. Although CD40 agonist can stimulate various APC populations, we observed that cDC1s were required for this CD40 agonist-induced priming (Fig. 6H). Protection by CD40 agonist monotherapy following either i.p. or orthotopic PDAC.Ova tumor challenge was abrogated in *Batf3*$^{-/-}$ mice lacking cDC1s (Fig. 6A-C). These results demonstrate that CD40 agonist-treatment acts through cDC1s to promote T-cell immunity and prevent escape of antigenic tumors within the pancreas and peritoneum.

CD40 agonist promotes epitope spread and enhances immune memory

To test whether the actions of CD40 agonism on cDC1s might also broaden the specificity of antitumor T-cell responses, we utilized mixing experiments with Ova^+ and Ova^- tumor cells. When WT mice were challenged s.c. with an 80:20 mixture of PDAC.Ova and parental PDAC C10, respectively, and treated on day 7 with control Ig, we observed progressive tumor growth (Fig. 7A-B), although the kinetics of growth were mildly delayed compared to T cell-depleted mice, which we previously showed is associated with a T cell-dependent elimination of the Ova^+ tumor fraction (41). Yet, if WT mice were instead treated with the CD40 agonist on day 7, we found that mixed tumors were controlled, and in many cases rejected completely, an effect which required the actions of both T cells and cDC1s (Fig. 7A-B). Immune elimination of Ova^- tumor cells was antigen-specific and not explained by a bystander effect within the TME because WT mice challenged with Ova^+ and Ova^- tumor cells on opposite flanks displayed a similar phenotype (Fig. 7C). These results thus directly establish the ability of CD40 agonism to broaden the antitumor T-cell repertoire by inducing epitope spread within antigenically heterogeneous tumors. When we challenged mice with s.c. parental PDAC following an initial priming with PDAC.Ova plus either control Ig or CD40 agonist treatment on day 7, we observed substantial differences in tumor outgrowth (Fig. 7D), underscoring the development of immune memory to shared (non-Ova) antigens and the enhancement of T-cell memory generation by CD40 agonist treatment.

Discussion

Identifying key determinants of tumor immunogenicity is critical to understanding immune escape and immunotherapy resistance. Although the TME of pancreatic cancer is presumed to be highly immunosuppressive, the extent to which such properties are orchestrated primarily by tumor cell-intrinsic biology versus the tissue microenvironment is difficult to ascertain. In this study, we used a clonal PDAC cell line with high antigenicity via enforced neoantigen expression to explore T cell-mediated immune surveillance. PDAC.Ova tumor cells were immunogenic and readily eliminated following s.c. or i.v. challenge, yet we unexpectedly observed immune escape within specific tissues such as the pancreas and peritoneum. Tumor outgrowth was not due to neoantigen loss or tumor-intrinsic editing, but rather reflected diminished $CD8^+$ T-cell priming and reduced immunogenicity of i.p. and orthotopic PDAC.Ova tumors. Thus, there is differential immune surveillance at distinct host tissue sites. We additionally found qualitative differences in the antitumor response, including a disparate requirement for $CD4^+$ T-cell help for control of orthotopic versus s.c. tumors and divergent growth of i.p. and s.c. tumor cells after concurrent challenge.

Our findings add to emerging evidence that antitumor immunity is shaped by host tissue determinants in addition to tumor cell-intrinsic factors (29). Prior studies in autochthonous models of cancer formation have suggested differential immune surveillance of neoantigen-expressing tumors based on the tissue of origin. For example, in sarcomas initiated by oncogenic Kras and p53 loss, T-cell surveillance inhibits tumor development and leads to immune escape with neoantigen loss (6), but lung adenocarcinomas, initiated by similar driver mutations and harboring the same neoantigens, develop with only delayed kinetics and retain neoantigen expression (52). A study in the KPC model of pancreatic cancer

shows that neoantigen expression in pancreatic epithelium accelerates premalignant lesion formation, PDAC development, and liver metastases, which was associated with the induction of a pathogenic T_H17 $CD4^+$ T-cell response (53). In contrast, expression of the same neoantigens during lung adenocarcinoma development elicits protective immunity with partial neoantigen loss (53).

Although autochthonous GEMMs have advantages over transplantable models, additional poorly defined genetic alterations are required for oncogenesis, and the activation (or inactivation) of divergent signaling pathways may be required for tumor formation at various tissue sites. Such differences could, in turn, contribute to the distinct immunobiology of Kras-driven tumors within different tissues. In the present study, we have eliminated such confounders by employing a clonal PDAC cell line to specifically interrogate the influence of the tissue microenvironment on T-cell surveillance of the same antigenic tumor. Limitations of this model system include reliance on a single dominant neoantigen, relative to the poorly characterized and likely variable number and strength of tumor antigens in humans, although in some cases responses appear to be dominated by a limited set of neoantigen-specific T cells (54). Additional limitations include those inherent in transplantable models, which require implantation site trauma and involve more accelerated tumor progression. Recognizing such limitations, our findings nevertheless reveal an important contribution of the host tissue microenvironment on immune surveillance, independent of tumor-intrinsic pathways. Potential relevance to mixed immunotherapy responses in human cancer patients warrants further study, particularly given divergent tumor-immune profiles identified in different metastatic lesions within the same patient, independent of genetic heterogeneity (25,55).

Mechanistically, we found that escape of PDAC.Ova tumors was associated with diminished priming of tumor-specific T cells, which required cDC1s, as well as CD40 signaling, but was independent of NK cells and the CXCR3-chemokine axis, in contrast to other tumor models (48–50). Consistent with a defect in T-cell priming, we demonstrated that either antecedent challenge with s.c. PDAC.Ova or a single dose of an anti-CD40 agonist prevented escape of i.p. and orthotopic PDAC.Ova tumors. The CD40 agonist acted through cDC1s to augment cross-priming of $CD8^+$ T cells, and through mixing experiments with Ova^+ and Ova^- tumor cells, we directly established that CD40 agonism could also promote epitope spread. In contrast, enhancing T-cell function alone via blockade of inhibitory receptors was not sufficient to restore protective immunity. PDAC.Ova tumors developing after orthotopic or i.p. injection, including tumors emerging with PD-1 blockade, retained neoantigen and MHC expression and showed no evidence of immunoediting.

Our findings differ from a prior study showing efficacy of PD-1/PD-L1 pathway blockade in neoantigen-expressing transplantable PDAC, with emergence of escape variants harboring MHC loss (56). Yet, they are consistent with other work finding no efficacy for checkpoint blockade in control of autochthonous Ova-expressing PDAC (53). This latter study also demonstrated decreased cDC infiltration and function in developing pancreatic tumors compared to lung tumors, which was unaffected by neoantigen expression and present in pre-malignant lesions, thus likely related to the tissue microenvironment (53). We have also previously shown that cDC dysfunction occurs early during the premalignant stages

of pancreatic tumorigenesis in KPC mice, which is linked to increased cDC1 apoptosis in the setting of elevated IL-6 (43). In the present study, we did not find evidence of diminished cDC1 infiltration into i.p. or orthotopic PDAC.Ova tumors compared to s.c. tumors; however, poor $CD8^+$ T-cell priming and its rescue with CD40 agonist-treatment was consistent with cDC1 dysfunction. Maturation marker expression on cDC1s was also largely unchanged, yet complex molecular programs (potentially dissociated from surface marker expression) likely distinguish immunogenic versus tolerogenic cDC1s, and characterizing functional subsets remains challenging (57,58). We hypothesize that microenvironmental cues at different anatomic sites influence cDC1 functionality and further investigation is warranted.

In conclusion, our study provides several important, novel insights about the immunobiology of pancreatic cancer. We showed that immune escape of antigenic tumors can occur without immunoediting and depends on the tissue site, with outgrowth of neoantigen-expressing PDAC occurring in the pancreas and peritoneum, despite high immunogenicity after s.c. or i.v. challenge. Tumor outgrowth at such sites neither required tumor-intrinsic editing nor could be prevented by augmenting T-cell effector function through PD-1 or CTLA-4 checkpoint blockade. Instead, immune escape was associated with diminished $CD8^+$ T-cell priming by cDC1s, without evidence of decreased DC infiltration or trafficking. Immunologic control at otherwise refractory sites was restored by enhancing cDC1 cross-presentation via CD40 agonist treatment, which promoted T-cell priming and broadened T-cell responses through epitope spread. Further understanding the host tissue determinants of cancer immunogenicity will thus be required to design improved combination immunotherapies for refractory solid tumors.

Supplementary Material

Refer to Web version on PubMed Central for supplementary material.

Acknowledgements

The authors wish to thank members of the laboratories of Dr. Robert Vonderheide and Dr. Ben Stanger for helpful discussions, and acknowledge funding support from NIH grants K12 CA076931 (M.S.D.), K08 CA241084 (M.S.D.), R01 CA229803 (R.H.V.), and the Parker Institute for Cancer Immunotherapy (R.H.V.).

Financial support: NIH grants K12 CA076931 (M.S.D.), K08 CA241084 (M.S.D.), R01 CA229803 (R.H.V.), and the Parker Institute for Cancer Immunotherapy (R.H.V.).

Conflict of interest statement: Dr. Vonderheide reports having received consulting fees or honoraria from Celldex, Lilly, Medimmune, and Verastem; and research funding from Apexigen, Fibrogen, Inovio, Janssen, and Lilly. He is an inventor on a licensed patent relating to cancer cellular immunotherapy and receives royalties from Children's Hospital Boston for a licensed research-only monoclonal antibody.

References

1. Ribas A, Wolchok JD. Cancer immunotherapy using checkpoint blockade. Science 2018;359(6382):1350–5 doi 10.1126/science.aar4060. [PubMed: 29567705]
2. Sharma P, Allison JP. The future of immune checkpoint therapy. Science 2015;348(6230):56–61 doi 10.1126/science.aaa8172. [PubMed: 25838373]

3. Schreiber RD, Old LJ, Smyth MJ. Cancer immunoediting: integrating immunity's roles in cancer suppression and promotion. Science 2011;331(6024):1565–70 doi 10.1126/science.1203486. [PubMed: 21436444]
4. Shankaran V, Ikeda H, Bruce AT, White JM, Swanson PE, Old LJ, et al. IFNgamma and lymphocytes prevent primary tumour development and shape tumour immunogenicity. Nature 2001;410(6832):1107–11 doi 10.1038/35074122. [PubMed: 11323675]
5. Matsushita H, Vesely MD, Koboldt DC, Rickert CG, Uppaluri R, Magrini VJ, et al. Cancer exome analysis reveals a T-cell-dependent mechanism of cancer immunoediting. Nature 2012;482(7385):400–4 doi 10.1038/nature10755. [PubMed: 22318521]
6. DuPage M, Mazumdar C, Schmidt LM, Cheung AF, Jacks T. Expression of tumour-specific antigens underlies cancer immunoediting. Nature 2012;482(7385):405–9 doi 10.1038/nature10803. [PubMed: 22318517]
7. Gubin MM, Zhang X, Schuster H, Caron E, Ward JP, Noguchi T, et al. Checkpoint blockade cancer immunotherapy targets tumour-specific mutant antigens. Nature 2014;515(7528):577–81 doi 10.1038/nature13988. [PubMed: 25428507]
8. Alspach E, Lussier DM, Miceli AP, Kizhvatov I, DuPage M, Luoma AM, et al. MHC-II neoantigens shape tumour immunity and response to immunotherapy. Nature 2019;574(7780):696–701 doi 10.1038/s41586-019-1671-8. [PubMed: 31645760]
9. Rizvi NA, Hellmann MD, Snyder A, Kvistborg P, Makarov V, Havel JJ, et al. Cancer immunology. Mutational landscape determines sensitivity to PD-1 blockade in non-small cell lung cancer. Science 2015;348(6230):124–8 doi 10.1126/science.aaa1348. [PubMed: 25765070]
10. Cristescu R, Mogg R, Ayers M, Albright A, Murphy E, Yearley J, et al. Pan-tumor genomic biomarkers for PD-1 checkpoint blockade-based immunotherapy. Science 2018;362(6411) doi 10.1126/science.aar3593.
11. Zaretsky JM, Garcia-Diaz A, Shin DS, Escuin-Ordinas H, Hugo W, Hu-Lieskovan S, et al. Mutations Associated with Acquired Resistance to PD-1 Blockade in Melanoma. N Engl J Med 2016;375(9):819–29 doi 10.1056/NEJMoa1604958. [PubMed: 27433843]
12. Anagnostou V, Smith KN, Forde PM, Niknafs N, Bhattacharya R, White J, et al. Evolution of Neoantigen Landscape during Immune Checkpoint Blockade in Non-Small Cell Lung Cancer. Cancer Discov 2017;7(3):264–76 doi 10.1158/2159-8290.CD-16-0828. [PubMed: 28031159]
13. McGranahan N, Rosenthal R, Hiley CT, Rowan AJ, Watkins TBK, Wilson GA, et al. Allele-Specific HLA Loss and Immune Escape in Lung Cancer Evolution. Cell 2017;171(6):1259–71 e11 doi 10.1016/j.cell.2017.10.001.
14. Topalian SL, Taube JM, Anders RA, Pardoll DM. Mechanism-driven biomarkers to guide immune checkpoint blockade in cancer therapy. Nat Rev Cancer 2016;16(5):275–87 doi 10.1038/nrc.2016.36. [PubMed: 27079802]
15. Fridman WH, Zitvogel L, Sautes-Fridman C, Kroemer G. The immune contexture in cancer prognosis and treatment. Nat Rev Clin Oncol 2017;14(12):717–34 doi 10.1038/nrclinonc.2017.101. [PubMed: 28741618]
16. Ott PA, Bang YJ, Piha-Paul SA, Razak ARA, Bennouna J, Soria JC, et al. T-Cell-Inflamed Gene-Expression Profile, Programmed Death Ligand 1 Expression, and Tumor Mutational Burden Predict Efficacy in Patients Treated With Pembrolizumab Across 20 Cancers: KEYNOTE-028. J Clin Oncol 2019;37(4):318–27 doi 10.1200/JCO.2018.78.2276. [PubMed: 30557521]
17. Spranger S, Luke JJ, Bao R, Zha Y, Hernandez KM, Li Y, et al. Density of immunogenic antigens does not explain the presence or absence of the T-cell-inflamed tumor microenvironment in melanoma. Proc Natl Acad Sci U S A 2016;113(48):E7759-E68 doi 10.1073/pnas.1609376113.
18. Spranger S, Gajewski TF. Impact of oncogenic pathways on evasion of antitumour immune responses. Nat Rev Cancer 2018;18(3):139–47 doi 10.1038/nrc.2017.117. [PubMed: 29326431]
19. Wellenstein MD, de Visser KE. Cancer-Cell-Intrinsic Mechanisms Shaping the Tumor Immune Landscape. Immunity 2018;48(3):399–416 doi 10.1016/j.immuni.2018.03.004. [PubMed: 29562192]
20. Pitt JM, Vetizou M, Daillere R, Roberti MP, Yamazaki T, Routy B, et al. Resistance Mechanisms to Immune-Checkpoint Blockade in Cancer: Tumor-Intrinsic and -Extrinsic Factors. Immunity 2016;44(6):1255–69 doi 10.1016/j.immuni.2016.06.001. [PubMed: 27332730]

21. Helmink BA, Khan MAW, Hermann A, Gopalakrishnan V, Wargo JA. The microbiome, cancer, and cancer therapy. Nat Med 2019;25(3):377–88 doi 10.1038/s41591-019-0377-7. [PubMed: 30842679]

22. Tumeh PC, Hellmann MD, Hamid O, Tsai KK, Loo KL, Gubens MA, et al. Liver Metastasis and Treatment Outcome with Anti-PD-1 Monoclonal Antibody in Patients with Melanoma and NSCLC. Cancer Immunol Res 2017;5(5):417–24 doi 10.1158/2326-6066.CIR-16-0325. [PubMed: 28411193]

23. Rosenberg JE, Hoffman-Censits J, Powles T, van der Heijden MS, Balar AV, Necchi A, et al. Atezolizumab in patients with locally advanced and metastatic urothelial carcinoma who have progressed following treatment with platinum-based chemotherapy: a single-arm, multicentre, phase 2 trial. Lancet 2016;387(10031):1909–20 doi 10.1016/S0140-6736(16)00561-4. [PubMed: 26952546]

24. Gerlinger M, Rowan AJ, Horswell S, Math M, Larkin J, Endesfelder D, et al. Intratumor heterogeneity and branched evolution revealed by multiregion sequencing. N Engl J Med 2012;366(10):883–92 doi 10.1056/NEJMoa1113205. [PubMed: 22397650]

25. Zhang AW, McPherson A, Milne K, Kroeger DR, Hamilton PT, Miranda A, et al. Interfaces of Malignant and Immunologic Clonal Dynamics in Ovarian Cancer. Cell 2018;173(7):1755–69 e22 doi 10.1016/j.cell.2018.03.073.

26. Rosenthal R, Cadieux EL, Salgado R, Bakir MA, Moore DA, Hiley CT, et al. Neoantigen-directed immune escape in lung cancer evolution. Nature 2019;567(7749):479–85 doi 10.1038/s41586-019-1032-7. [PubMed: 30894752]

27. DuPage M, Jacks T. Genetically engineered mouse models of cancer reveal new insights about the antitumor immune response. Curr Opin Immunol 2013;25(2):192–9 doi 10.1016/j.coi.2013.02.005. [PubMed: 23465466]

28. Vonderheide RH. The Immune Revolution: A Case for Priming, Not Checkpoint. Cancer Cell 2018;33(4):563–9 doi 10.1016/j.ccell.2018.03.008. [PubMed: 29634944]

29. Salmon H, Remark R, Gnjatic S, Merad M. Host tissue determinants of tumour immunity. Nat Rev Cancer 2019;19(4):215–27 doi 10.1038/s41568-019-0125-9. [PubMed: 30867580]

30. Morrison AH, Byrne KT, Vonderheide RH. Immunotherapy and Prevention of Pancreatic Cancer. Trends Cancer 2018;4(6):418–28 doi 10.1016/j.trecan.2018.04.001. [PubMed: 29860986]

31. Royal RE, Levy C, Turner K, Mathur A, Hughes M, Kammula US, et al. Phase 2 trial of single agent Ipilimumab (anti-CTLA-4) for locally advanced or metastatic pancreatic adenocarcinoma. J Immunother 2010;33(8):828–33 doi 10.1097/CJI.0b013e3181eec14c. [PubMed: 20842054]

32. Brahmer JR, Tykodi SS, Chow LQ, Hwu WJ, Topalian SL, Hwu P, et al. Safety and activity of anti-PD-L1 antibody in patients with advanced cancer. N Engl J Med 2012;366(26):2455–65 doi 10.1056/NEJMoa1200694. [PubMed: 22658128]

33. Biankin AV, Waddell N, Kassahn KS, Gingras MC, Muthuswamy LB, Johns AL, et al. Pancreatic cancer genomes reveal aberrations in axon guidance pathway genes. Nature 2012;491(7424):399–405 doi 10.1038/nature11547. [PubMed: 23103869]

34. Ino Y, Yamazaki-Itoh R, Shimada K, Iwasaki M, Kosuge T, Kanai Y, et al. Immune cell infiltration as an indicator of the immune microenvironment of pancreatic cancer. Br J Cancer 2013;108(4):914–23 doi 10.1038/bjc.2013.32. [PubMed: 23385730]

35. Balachandran VP, Luksza M, Zhao JN, Makarov V, Moral JA, Remark R, et al. Identification of unique neoantigen qualities in long-term survivors of pancreatic cancer. Nature 2017;551(7681):512–6 doi 10.1038/nature24462. [PubMed: 29132146]

36. Balli D, Rech AJ, Stanger BZ, Vonderheide RH. Immune Cytolytic Activity Stratifies Molecular Subsets of Human Pancreatic Cancer. Clin Cancer Res 2017;23(12):3129–38 doi 10.1158/1078-0432.CCR-16-2128. [PubMed: 28007776]

37. Rooney MS, Shukla SA, Wu CJ, Getz G, Hacohen N. Molecular and genetic properties of tumors associated with local immune cytolytic activity. Cell 2015;160(1–2):48–61 doi 10.1016/j.cell.2014.12.033. [PubMed: 25594174]

38. Bayne LJ, Beatty GL, Jhala N, Clark CE, Rhim AD, Stanger BZ, et al. Tumor-derived granulocyte-macrophage colony-stimulating factor regulates myeloid inflammation and T cell immunity

in pancreatic cancer. Cancer Cell 2012;21(6):822–35 doi 10.1016/j.ccr.2012.04.025. [PubMed: 22698406]

39. Feig C, Jones JO, Kraman M, Wells RJ, Deonarine A, Chan DS, et al. Targeting CXCL12 from FAP-expressing carcinoma-associated fibroblasts synergizes with anti-PD-L1 immunotherapy in pancreatic cancer. Proc Natl Acad Sci U S A 2013;110(50):20212–7 doi 10.1073/pnas.1320318110.
40. Li J, Byrne KT, Yan F, Yamazoe T, Chen Z, Baslan T, et al. Tumor Cell-Intrinsic Factors Underlie Heterogeneity of Immune Cell Infiltration and Response to Immunotherapy. Immunity 2018;49(1):178–93 e7 doi 10.1016/j.immuni.2018.06.006.
41. Evans RA, Diamond MS, Rech AJ, Chao T, Richardson MW, Lin JH, et al. Lack of immunoediting in murine pancreatic cancer reversed with neoantigen. JCI Insight 2016;1(14) doi 10.1172/jci.insight.88328.
42. Byrne KT, Vonderheide RH. CD40 Stimulation Obviates Innate Sensors and Drives T Cell Immunity in Cancer. Cell Rep 2016;15(12):2719–32 doi 10.1016/j.celrep.2016.05.058. [PubMed: 27292635]
43. Lin JH, Huffman AP, Wattenberg MM, Walter DM, Carpenter EL, Feldser DM, et al. Type 1 conventional dendritic cells are systemically dysregulated early in pancreatic carcinogenesis. J Exp Med 2020;217(8) doi 10.1084/jem.20190673.
44. Pylayeva-Gupta Y, Das S, Handler JS, Hajdu CH, Coffre M, Koralov SB, et al. IL35-Producing B Cells Promote the Development of Pancreatic Neoplasia. Cancer Discov 2016;6(3):247–55 doi 10.1158/2159-8290.CD-15-0843. [PubMed: 26715643]
45. Lee KE, Spata M, Bayne LJ, Buza EL, Durham AC, Allman D, et al. Hif1a Deletion Reveals Pro-Neoplastic Function of B Cells in Pancreatic Neoplasia. Cancer Discov 2016;6(3):256–69 doi 10.1158/2159-8290.CD-15-0822. [PubMed: 26715642]
46. Hildner K, Edelson BT, Purtha WE, Diamond M, Matsushita H, Kohyama M, et al. Batf3 deficiency reveals a critical role for CD8alpha+ dendritic cells in cytotoxic T cell immunity. Science 2008;322(5904):1097–100 doi 10.1126/science.1164206. [PubMed: 19008445]
47. Ferris ST, Durai V, Wu R, Theisen DJ, Ward JP, Bern MD, et al. cDC1 prime and are licensed by CD4(+) T cells to induce anti-tumour immunity. Nature 2020 doi 10.1038/s41586-020-2611-3.
48. Spranger S, Dai D, Horton B, Gajewski TF. Tumor-Residing Batf3 Dendritic Cells Are Required for Effector T Cell Trafficking and Adoptive T Cell Therapy. Cancer Cell 2017;31(5):711–23 e4 doi 10.1016/j.ccell.2017.04.003.
49. Mikucki ME, Fisher DT, Matsuzaki J, Skitzki JJ, Gaulin NB, Muhitch JB, et al. Non-redundant requirement for CXCR3 signalling during tumoricidal T-cell trafficking across tumour vascular checkpoints. Nat Commun 2015;6:7458 doi 10.1038/ncomms8458. [PubMed: 26109379]
50. Bottcher JP, Bonavita E, Chakravarty P, Blees H, Cabeza-Cabrerizo M, Sammicheli S, et al. NK Cells Stimulate Recruitment of cDC1 into the Tumor Microenvironment Promoting Cancer Immune Control. Cell 2018;172(5):1022–37 e14 doi 10.1016/j.cell.2018.01.004.
51. De Togni P, Goellner J, Ruddle NH, Streeter PR, Fick A, Mariathasan S, et al. Abnormal development of peripheral lymphoid organs in mice deficient in lymphotoxin. Science 1994;264(5159):703–7. [PubMed: 8171322]
52. DuPage M, Cheung AF, Mazumdar C, Winslow MM, Bronson R, Schmidt LM, et al. Endogenous T cell responses to antigens expressed in lung adenocarcinomas delay malignant tumor progression. Cancer Cell 2011;19(1):72–85 doi 10.1016/j.ccr.2010.11.011. [PubMed: 21251614]
53. Hegde S, Krisnawan VE, Herzog BH, Zuo C, Breden MA, Knolhoff BL, et al. Dendritic Cell Paucity Leads to Dysfunctional Immune Surveillance in Pancreatic Cancer. Cancer Cell 2020;37(3):289–307 e9 doi 10.1016/j.ccell.2020.02.008.
54. Kalaora S, Wolf Y, Feferman T, Barnea E, Greenstein E, Reshef D, et al. Combined Analysis of Antigen Presentation and T-cell Recognition Reveals Restricted Immune Responses in Melanoma. Cancer Discov 2018;8(11):1366–75 doi 10.1158/2159-8290.CD-17-1418. [PubMed: 30209080]
55. Jimenez-Sanchez A, Memon D, Pourpe S, Veeraraghavan H, Li Y, Vargas HA, et al. Heterogeneous Tumor-Immune Microenvironments among Differentially Growing Metastases in an Ovarian Cancer Patient. Cell 2017;170(5):927–38 e20 doi 10.1016/j.cell.2017.07.025.

56. Burrack AL, Spartz EJ, Raynor JF, Wang I, Olson M, Stromnes IM. Combination PD-1 and PD-L1 Blockade Promotes Durable Neoantigen-Specific T Cell-Mediated Immunity in Pancreatic Ductal Adenocarcinoma. Cell Rep 2019;28(8):2140–55 e6 doi 10.1016/j.celrep.2019.07.059.

57. Ardouin L, Luche H, Chelbi R, Carpentier S, Shawket A, Montanana Sanchis F, et al. Broad and Largely Concordant Molecular Changes Characterize Tolerogenic and Immunogenic Dendritic Cell Maturation in Thymus and Periphery. Immunity 2016;45(2):305–18 doi 10.1016/j.immuni.2016.07.019. [PubMed: 27533013]

58. Maier B, Leader AM, Chen ST, Tung N, Chang C, LeBerichel J, et al. A conserved dendritic-cell regulatory program limits antitumour immunity. Nature 2020;580(7802):257–62 doi 10.1038/s41586-020-2134-y. [PubMed: 32269339]

Synopsis:

Data show that tumor antigenicity is necessary, but not sufficient, for effective cancer immune surveillance. Neoantigen-expressing tumors can escape in certain host tissue microenvironments in the absence of immunoediting, despite displaying high tumor immunogenicity at other sites.

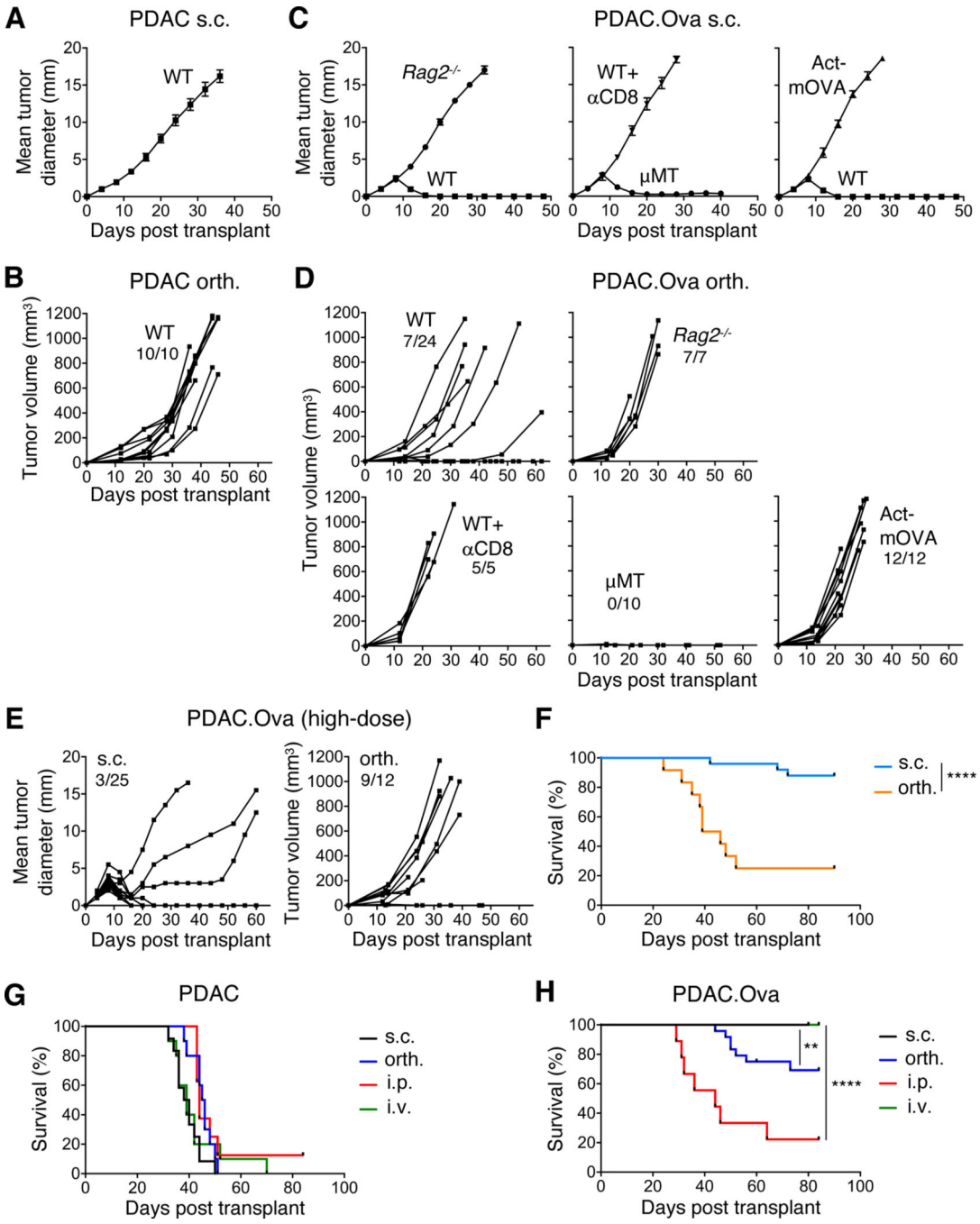

Figure 1. Selective outgrowth of neoantigen-expressing PDAC in pancreas and peritoneum.

(**A**-**B**) WT mice were challenged with 1.25×10^5 parental PDAC cells by s.c. (A) or orthotopic (orth.) (B) injection, and tumor growth is plotted as mean tumor diameter (±S.E.M) for n=8 mice in A, or tumor volumes by serial ultrasound for n=10 mice in B. (**C**-**D**) Cohorts of WT, *Rag2*$^{-/-}$, μMT, Act-mOVA, or WT mice treated with depleting anti-CD8 (n=4–15 mice/group) were injected s.c. (C) or orthotopically (D) with 1.25×10^5 PDAC.Ova cells, and tumor growth is shown. (**E**-**F**) Tumor growth and survival of WT mice injected s.c. or orthotopically with PDAC.Ova cells at a high-dose (1×10^6 cells/mouse),

with group sizes as indicated. (**G**-**H**) Survival curves of WT mice challenged with either PDAC (n=8–12 mice/group) (G) or PDAC.Ova (n=5–24 mice/group) (H) cells at 1.25×10^5 cells/mouse via s.c., orthotopic, i.p., or i.v. injection. ****p<0.0001; **p<0.01, by log-rank test.

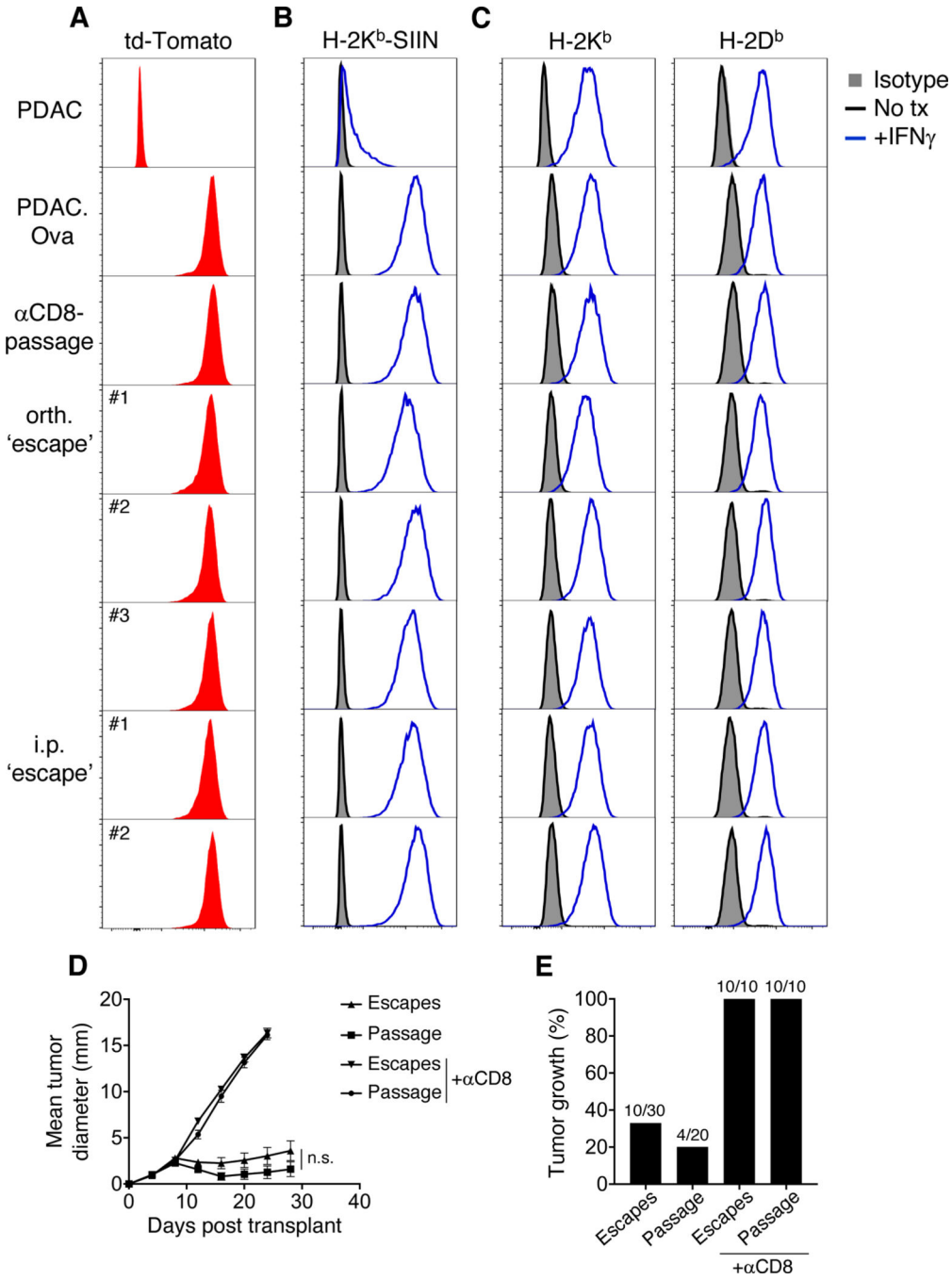

Figure 2. Immune escape of PDAC.Ova tumors is not due to neoantigen loss.

(**A-C**) Expression determined by flow cytometry of td-Tomato (A), SIINFEKL bound to H-2K^b (H-2K^b-SIIN) (B), and MHC class I (H-2K^b, H-2D^b) (C) are shown for PDAC, PDAC.Ova, a representative PDAC.Ova line after orthotopic (orth.) passage in an anti-CD8-treated WT mouse ('αCD8-passage'), and independent lines derived from orthotopic (n=3, orth. 'escape') or i.p. (n=2, i.p. 'escape') PDAC.Ova tumors in WT mice. For MHC staining, isotype control is shown in gray shaded histograms, untreated cells in black, and cells treated with IFNγ for 48 hours in blue. Data are representative of at least

3 independent experiments. (**D**-**E**) PDAC.Ova orthotopic ‘escape’ and ‘passage’ tumor lines were transplanted s.c. into naïve WT hosts (1.25×10^5 cells/mouse), and mean tumor diameter (±S.E.M) is shown in D, or percent tumor growth (>5 mm diameter by day 40) in E, for n=3 escape lines and n=4 passage lines transplanted into n=20–30 WT mice or n=10 anti-CD8-treated mice. Growth curve comparison between escape and passage tumors by two-way ANOVA; n.s., not significant.

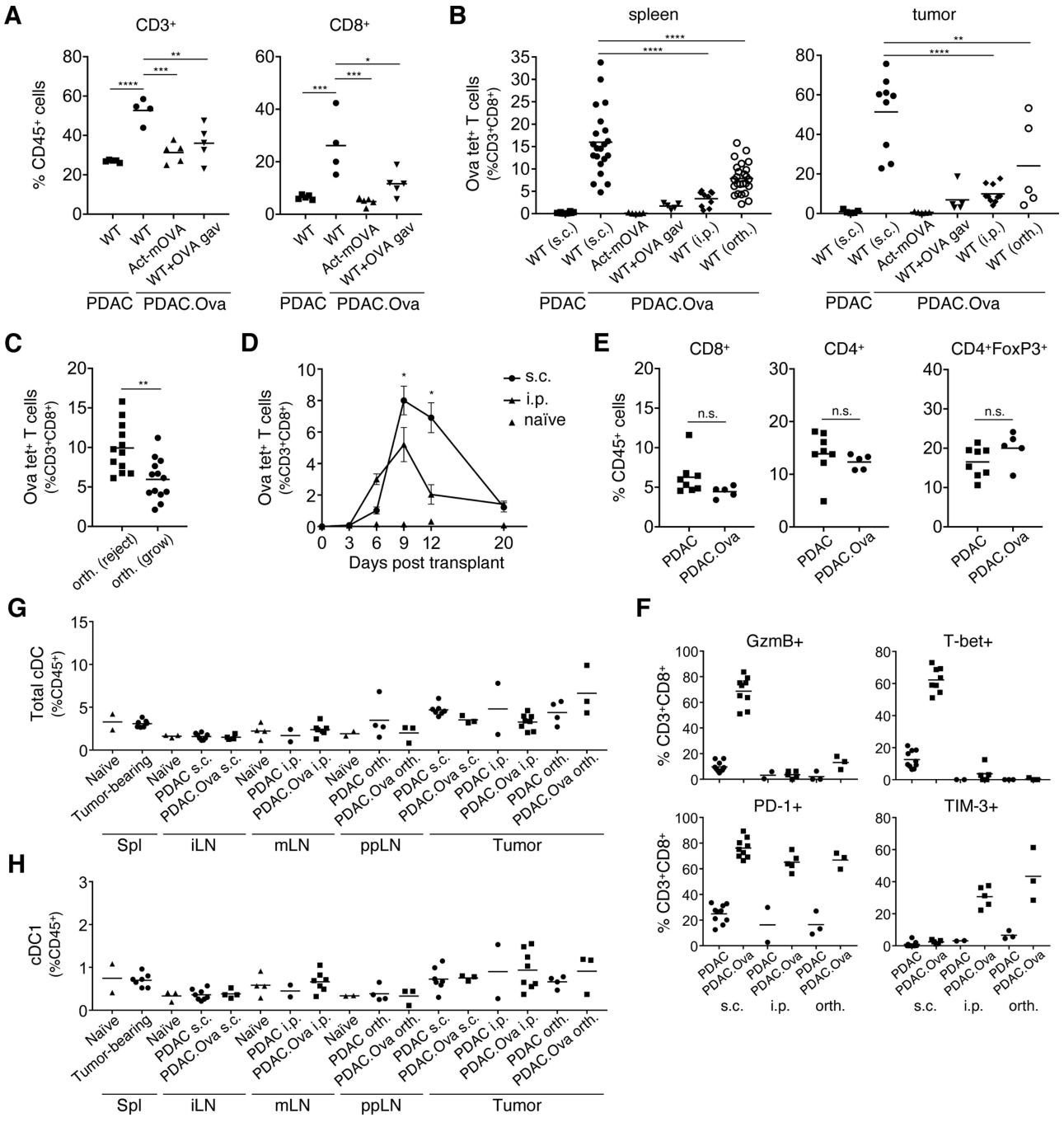

Figure 3. PDAC.Ova growth is associated with diminished T-cell priming.

(**A-B**) Groups of WT, Act-mOVA, and WT mice pretreated with Ova oral gavage were injected s.c., i.p., or orthotopically (orth.) with 1×10^6 PDAC or PDAC.Ova cells as indicated, and tumors or spleens were harvested at day 9 for flow cytometric analysis. T-cell subsets in the tumor for n=4–5 mice/group (A) or SIINFEKL-H-2K^b tetramer$^+$ (Ova tet$^+$) T cells in the tumor and spleen for n=5–25 mice/group (B) are shown. (**C**) Ova tet$^+$ T cells in the spleens of WT mice challenged with orthotopic PDAC.Ova from B (n=25) were subgrouped based on the presence of progressively growing tumor vs. no gross tumor

at harvest on day 12–14. (**D**) Ova tet^{+} T cells in the spleens of WT mice injected s.c. or i.p. with PDAC.Ova measured at the indicated time for n=5–10 mice/group, compared to naïve controls (n=2–4). Plot reflects percent of CD8^{+} T cells (±S.E.M), with significance at day 9 and 12 by Mann-Whitney test. (**E**) Late i.p. PDAC and PDAC.Ova tumors from WT mice (n=5–8 mice/group) were assayed for the indicated immune population. (**F**) CD8^{+} T cells isolated from s.c., i.p., or orthotopic PDAC and PDAC.Ova tumors (n=2–10 mice/group) were assayed for the indicated immune markers by flow cytometry. (**G**-**H**) Total cDC or cDC1s from spleen (Spl), tumor-draining inguinal lymph node (iLN), mesenteric LN (mLN), or peripancreatic LN (ppLN), and s.c., i.p., or orthotopic PDAC and PDAC.Ova tumors were measured, along with naïve WT controls, for n=2–8 mice/group. ****p<0.0001; ***p<0.001; **p<0.01; *p<0.05; n.s., not significant, by one-way ANOVA or unpaired t test. Data reflect at least 2 experiments with group sizes as indicated.

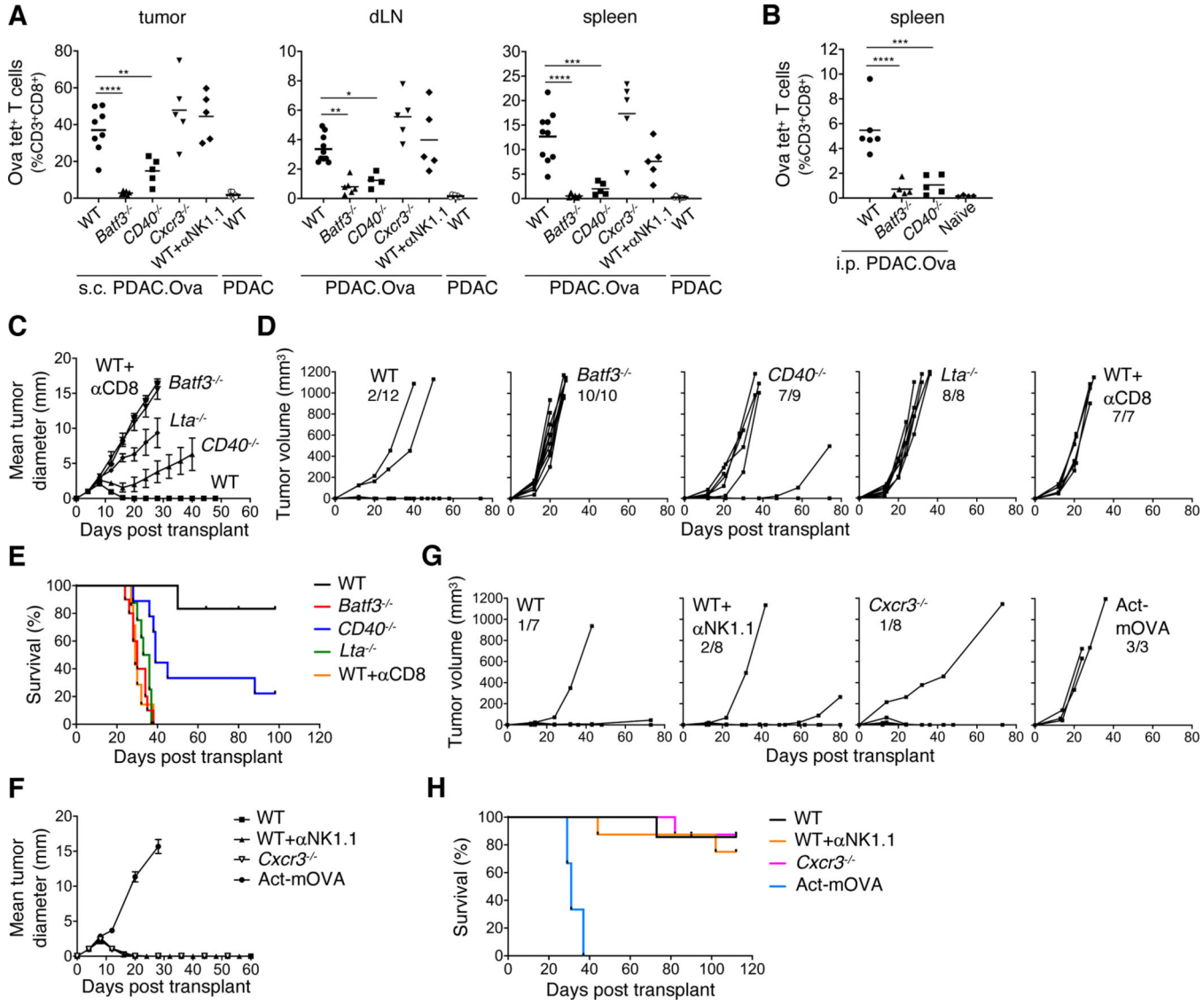

Figure 4. cDC1s and host CD40 are required for antitumor immunity, independent of NK cells and the CXCR3-chemokine axis.

(**A**) WT, *Batf3*$^{-/-}$, *CD40*$^{-/-}$, *Cxcr3*$^{-/-}$, and WT mice treated with anti-NK1.1 (n=5–10 mice/group) were injected s.c. with 1×10^6 PDAC.Ova or PDAC cells and tumors, dLNs, or spleens were harvested at day 9 and analyzed for Ova tet$^+$ T cells by flow cytometry. (**B**) Ova tet$^+$ T cells in the spleens at day 9 of WT, *Batf3*$^{-/-}$, and *CD40*$^{-/-}$ mice (n=5–6 mice/group) injected i.p. with 1×10^6 PDAC.Ova cells, compared to naïve WT controls (n=2). (**C-E**) Tumor growth and survival curves for cohorts of WT, *Batf3*$^{-/-}$, *CD40*$^{-/-}$, *Lta*$^{-/-}$, or anti-CD8-treated WT mice injected s.c. (C) or orthotopically (orth.) (D-E) with 1.25×10^5 PDAC.Ova cells. Plots represent mean tumor diameter (±S.E.M) for n=7–18 mice/group (C) or tumor volumes of individual mice with group sizes as shown (D). Survival curves from orthotopically injected mice are in E. (**F-H**) WT, *Cxcr3*$^{-/-}$, Act-mOVA, and WT mice treated with anti-NK1.1 were injected s.c. (F) or orthotopically (G-H) with 1.25×10^5 PDAC.Ova cells, and tumor growth was monitored. Data reflect mean tumor

diameter (±S.E.M) for n=3–5 mice/group (F) or tumor volumes of individual mice with indicated group sizes (G). Survival curves from orthotopically injected mice are in H. ****p<0.0001; ***p<0.001; **p<0.01; *p<0.05, by one-way ANOVA. Flow data include at least 2 experiments with group sizes as indicated.

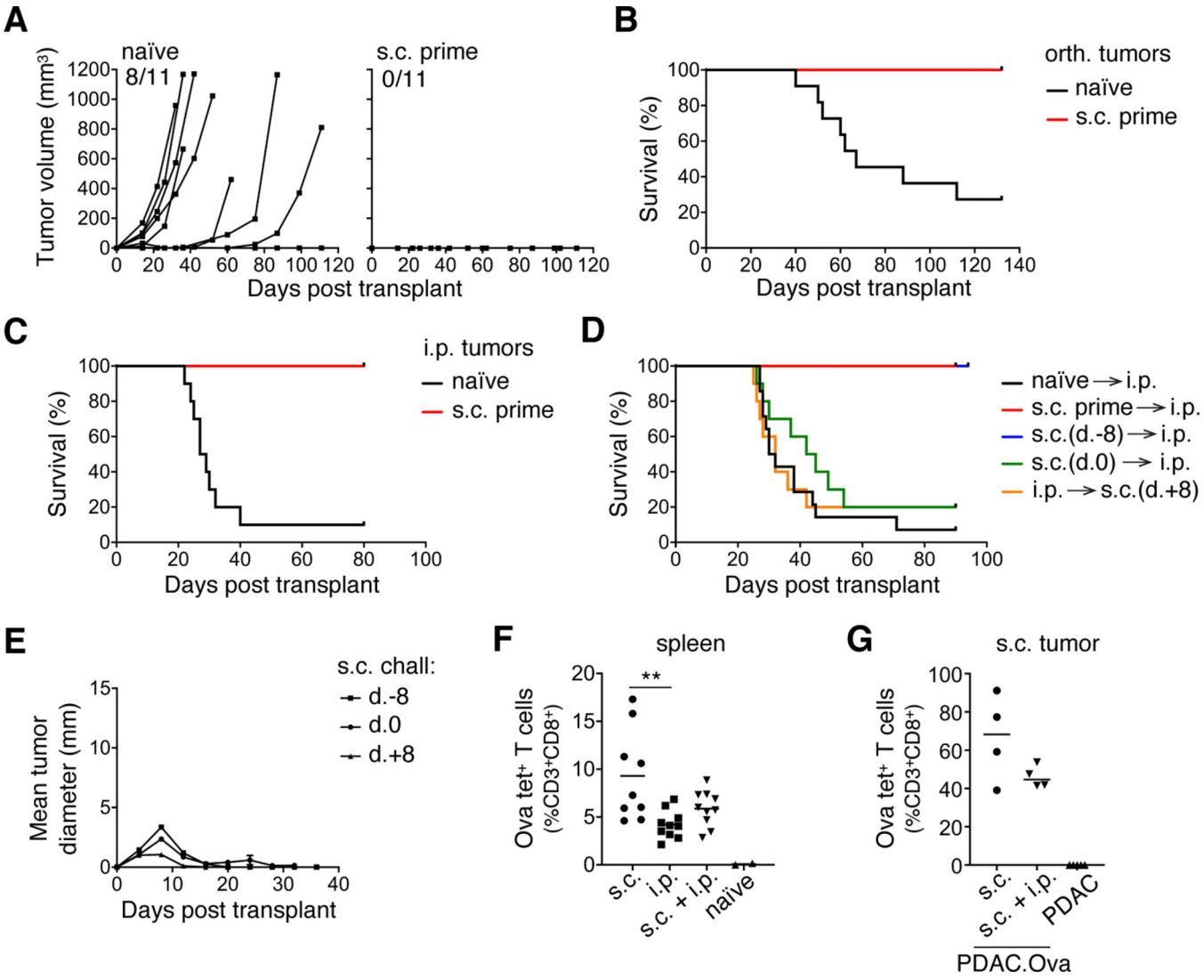

Figure 5. Protection by prior, but not concurrent, PDAC.Ova priming.

(**A**-**B**) Naïve WT mice or WT mice previously primed with s.c. PDAC.Ova (n=11 mice/group) were injected orthotopically (orth.) with 1×10^6 PDAC.Ova cells, and tumor growth was monitored by ultrasound. The corresponding survival curves are shown in B. (**C**) Survival curves from similar cohorts of mice (n=10–12 mice/group) challenged i.p. with 1×10^6 PDAC.Ova cells. (**D**) Survival of WT mice (n=10–14 mice/group) injected s.c. with PDAC.Ova cells at the indicated time point relative to i.p. challenge with 1×10^6 PDAC.Ova cells at day 0. (**E**) Growth kinetics of s.c. PDAC.Ova in mice from D. Data reflect mean tumor diameter ±S.E.M for n=10 mice/group and include s.c. PDAC.Ova challenge at 1×10^6 or 1.25×10^5 cells/mouse. (**F**-**G**) Spleens or s.c. tumors at day 9 were harvested from WT mice injected s.c., i.p., or both s.c. and i.p. with 1×10^6 PDAC.Ova cells (n=4–10 mice/group) and analyzed for Ova tet$^+$ T cells, with naïve or PDAC-injected control mice. **p<0.01, by one-way ANOVA. Flow data represent at least 2 experiments.

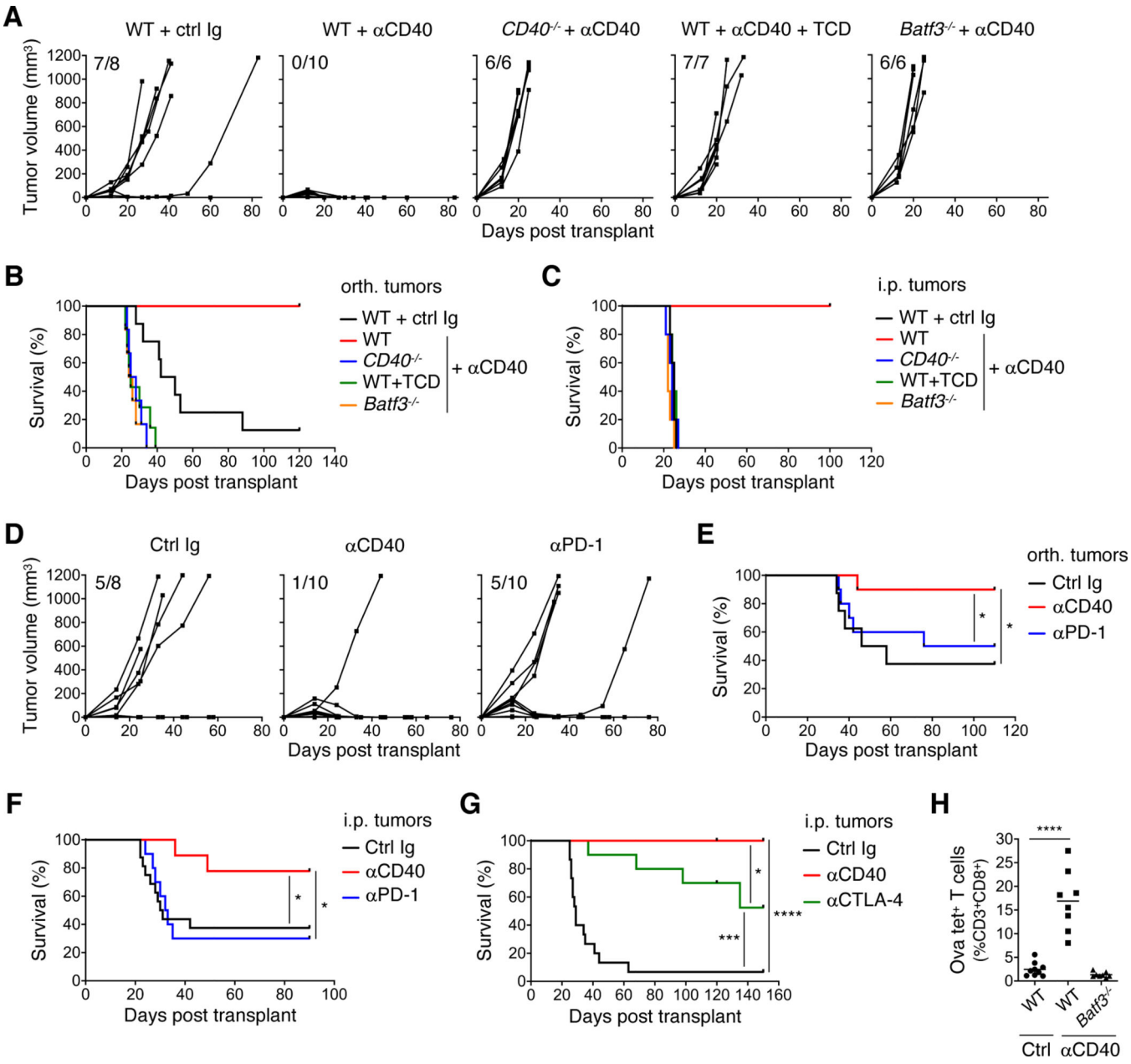

Figure 6. CD40 agonism, but not T-cell checkpoint blockade, prevents PDAC.Ova escape.

(**A**-**B**) Cohorts of WT, *CD40*$^{-/-}$, T cell-depleted (TCD) anti-CD4 and anti-CD8-treated WT mice, or *Batf3*$^{-/-}$ mice were injected orthotopically (orth.) with PDAC.Ova (1×10^6 cells/mouse) and treated at day 7 with a single dose of either ctrl Ig or agonistic anti-CD40. Tumor volumes by serial ultrasound for n=6–10 mice/group are shown in A, with corresponding survival curves in B. (**C**) Survival curves from similar cohorts of mice (n=5 mice/group) injected i.p. with PDAC.Ova and treated at day 7 with ctrl Ig or anti-CD40. (**D**-**E**) WT mice injected orthotopically with PDAC.Ova were treated at day 12 with ctrl Ig, CD40 agonist (single dose), or anti-PD-1 (3 doses, q3 days). Tumor volumes for n=8–10 mice/group are shown in D, with corresponding survival curves in E. (**F**) Survival curves of WT mice (n=9–16 mice/group) injected i.p. with PDAC.Ova and treated at day 11–12

with ctrl Ig, CD40 agonist, or anti-PD-1. (**G**) Survival curves of WT mice (n=10–15 mice/group) challenged i.p. with PDAC.Ova and treated at day 6–7 with ctrl Ig, CD40 agonist, or anti-CTLA-4 (3 doses, q3 days). (**H**) Spleens from WT or *Batf3*$^{-/-}$ mice (n=8–9 mice/group) injected i.p. with PDAC.Ova and treated at day 7 with ctrl Ig or CD40 agonist were harvested at day 12 for flow cytometric analysis of Ova tet^{+} T cells. ****p<0.0001; ***p<0.001, *p<0.05, by log-rank test or one-way ANOVA. Flow data reflect 3 independent experiments.

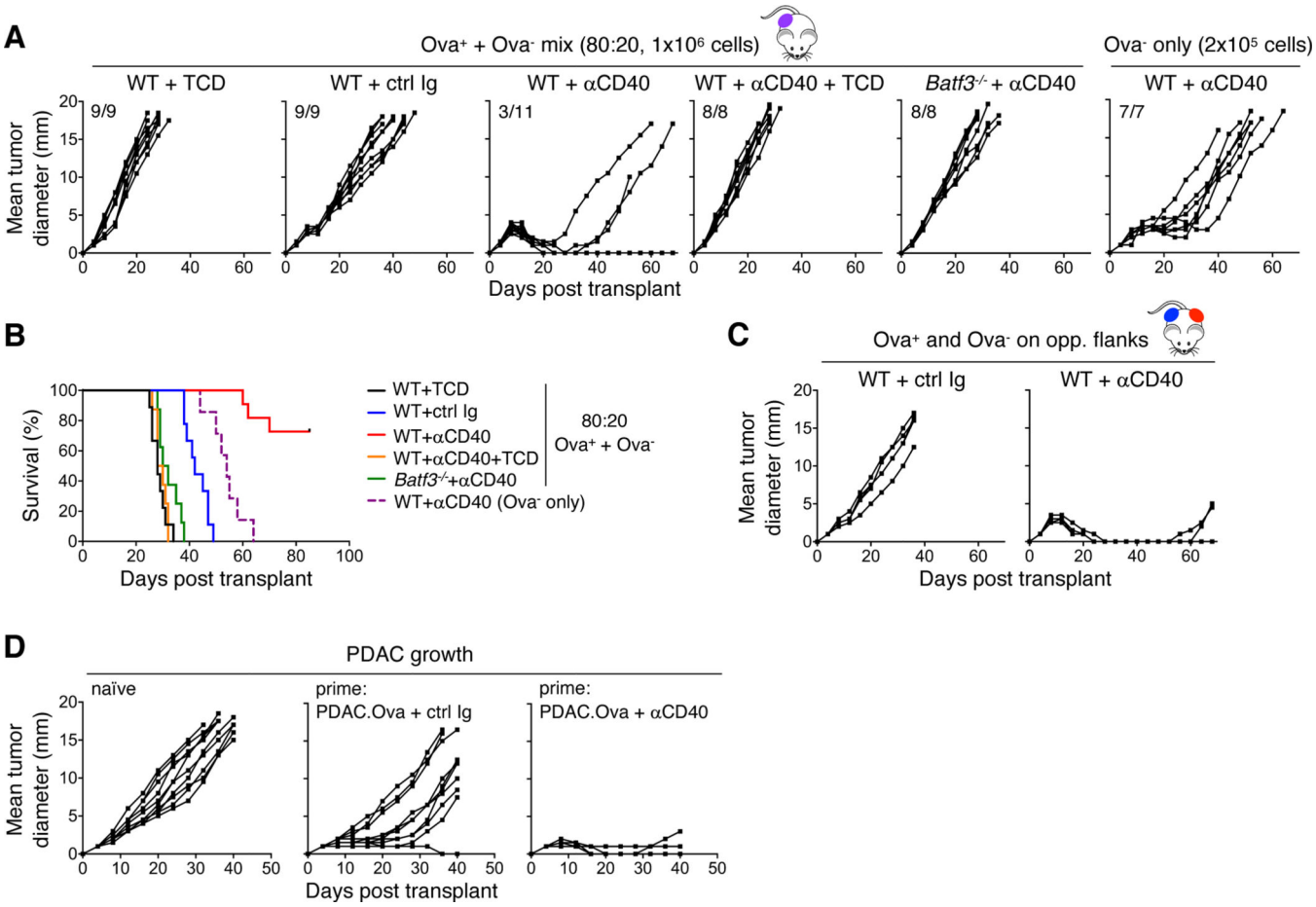

Figure 7. CD40 agonism promotes epitope spread and enhances immune memory.

(**A**-**B**) 80:20 mixtures (1×10^6 cells/mouse) of PDAC.Ova and parental PDAC clone C10 were injected s.c. into T cell-depleted (TCD) WT mice, WT, or *Batf3*$^{-/-}$ mice treated on day 7 with ctrl Ig or agonistic anti-CD40, or WT mice treated with CD40 agonism and concurrent TCD. WT mice challenged s.c. with 2×10^5 PDAC C10 alone and treated with CD40 agonist were included as a control. Growth curves from n=7–11 mice/group are shown, with the corresponding survival curves in B. (**C**) WT mice injected s.c. on opposite flanks with PDAC.Ova (8×10^5 cells) and PDAC C10 (2×10^5 cells) were treated on day 7 with either ctrl Ig or anti-CD40 agonist. Plots reflect growth kinetics of C10 tumors for n=5 mice/group. PDAC.Ova tumors on the opposite flank were rejected in all CD40 agonist-treated mice and 4/5 ctrl Ig-treated mice. (**D**) Naïve WT mice or mice previously challenged s.c. with 1×10^6 PDAC.Ova tumor cells and treated with ctrl Ig or CD40 agonist on day 7, were injected following tumor rejection (day 40 relative to PDAC.Ova) with 1.25×10^5 parental PDAC cells s.c. on the opposite flank and tumor growth was followed for n=10 mice/group.